Biomineralization

International Edition: DOI: 10.1002/anie.201507327
German Edition: DOI: 10.1002/ange.201507327

Insight into the Supramolecular Architecture of Intact Diatom Biosilica from DNP-Supported Solid-State NMR Spectroscopy

Anne Jantschke, Eline Koers, Deni Mance, Markus Weingarth, Eike Brunner, and Marc Baldus**

Abstract: *Diatom biosilica is an inorganic/organic hybrid with interesting properties. The molecular architecture of the organic material at the atomic and nanometer scale has so far remained unknown, in particular for intact biosilica. A DNP-supported ssNMR approach assisted by microscopy, MS, and MD simulations was applied to study the structural organization of intact biosilica. For the first time, the secondary structure elements of tightly biosilica-associated native proteins in diatom biosilica were characterized in situ. Our data suggest that these proteins are rich in a limited set of amino acids and adopt a mixture of random-coil and β-strand conformations. Furthermore, biosilica-associated long-chain polyamines and carbohydrates were characterized, thereby leading to a model for the supramolecular organization of intact biosilica.*

Biomineralization is the formation of inorganic materials by biological processes. Examples for calcium biomineralization are calcium phosphates like bones and calcium carbonates such as nacre or coccoliths. The most abundant silica biomineralization process occurs in diatoms, which are organisms of global ecological importance. Diatom biosilica is an inorganic/organic hybrid with significant potential for novel (bio)material science applications.[1] Diatom cell walls exhibit species-specific micro- and nano-patterning. They typically contain 1–15 wt.%[2] of tightly bound organic molecules.[3] The chemical structure and composition of the silica-attached organic material is partly known. However, its structural organization at the atomic and nanometer scales has remained elusive, in particular for intact biosilica. So far, structural studies of biomineral-associated proteins have been limited to samples prepared in vitro.[4] To deal with the spectroscopic challenges related to examining intact biominerals, we applied a dynamic nuclear polarization (DNP)-supported solid-state NMR (ssNMR) approach assisted by microscopy, mass spectrometry (MS), and molecular dynamics (MD) simulations. We were thus able to characterize in situ the secondary structure elements of tightly biosilica-associated native proteins in fully [^{13}C, ^{15}N, ^{29}Si]-enriched intact diatom biosilica from *Stephanopyxis turris*. Furthermore, we were able to characterize biosilica-associated long-chain polyamines (LCPAs) and carbohydrates. Taken together, our experiments enabled us to establish a model for the supramolecular arrangement of intact biosilica.

We investigated fully [^{13}C, ^{15}N, ^{29}Si]-isotope-enriched diatom biosilica from *Stephanopyxis turris* before and after extraction with sodium dodecyl sulfate (SDS)/ethylenediaminetetraacetic acid (EDTA) by bright-field and helium-ion microscopy. Figure 1a shows a bright-field micrograph of living *S. turris*. A silica-based cell wall surrounds the algal cell. While biosilica remains intact after SDS/EDTA treatment (Figure 1b,c), all other cell constituents are removed. Diatom biosilica is a low-surface-area material with a BET surface of approximately 20–30 m^2g^{-1} (BET: Brunauer–Emmett–Teller, Section S1 in the Supporting Information) for *S. turris*. It still contains a significant amount of strongly silica-associated biomolecules ($\approx$15 wt.%).[2] Note the elaborate structure of the biosilica, which resembles a "lightweight construction".

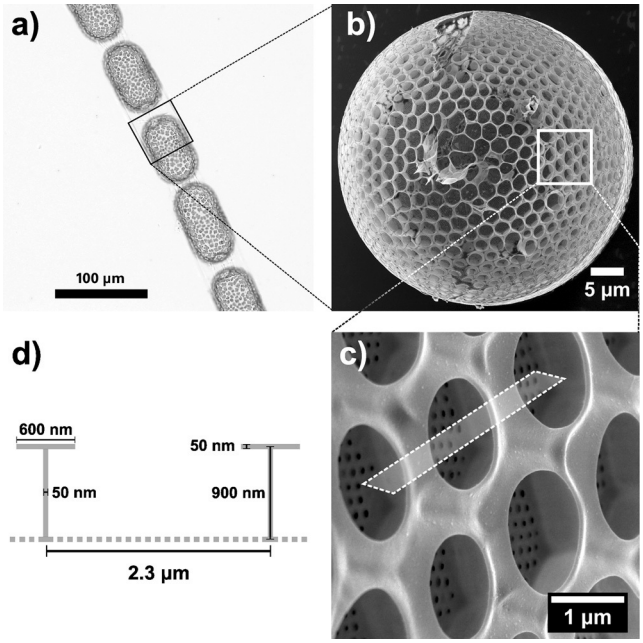

Figure 1. Biosilica: a micro- and nanopatterned hybrid material. a) Bright-field microscopy image of *S. turris* (living cells). b,c) Helium-ion microscopy images of *S. turris* biosilica extracted by treatment with SDS/EDTA. The gray rectangle in (c) indicates a region for which a cut through the cell wall would reveal the characteristic profile schematically depicted in (d).

[*] Dr. A. Jantschke,[+] Prof. E. Brunner
Bioanalytical Chemistry, TU Dresden
Bergstraße 66, 01069 Dresden (Germany)
E-mail: eike.brunner@tu-dresden.de
Dr. E. Koers,[+] D. Mance, Dr. M. Weingarth, Prof. M. Baldus
NMR Spectroscopy, Bijvoet Center for Biomolecular Research
Utrecht University
Padualaan 8, 3584 CH Utrecht (The Netherlands)
E-mail: m.baldus@uu.nl
[+] These authors contributed equally to this work.

Supporting information (including experimental details) and ORCID(s) from the author(s) for this article are available on the WWW under http://dx.doi.org/10.1002/anie.201507327.

Characteristic dimensions are given in Figure 1 d. The thickness of individual silica layers making up these lightweight structures typically amounts to approximately 50 nm.

Over the past 15 years, extensive research work has led to the identification of strongly biosilica-associated biomolecules. Dissolution of the silica followed by fractionation enabled the identification of various soluble and insoluble organic components such as LCPAs,[3a] as well as special protein families such as silaffins,[3b] silacidins,[3c] and cingulins.[3d] These biomolecules are potentially involved in the silica formation process.[3a–d,g,h] Carbohydrates were also found to be strongly associated with the biosilica.[3e–h] They may also be attached to silica-bound proteins in the form of glycoproteins.

Solid-state NMR (ssNMR) is a well-established method for the characterization of various types of materials and complex biomolecules, including inorganic/organic hybrids such as biominerals.[4,5] Spectroscopic sensitivity and adequate spectral resolution are critical for the characterization of surface functionalities and the inorganic/organic interfaces. To obtain insight into the structural organization of *S. turris* biosilica, we resorted to DNP-supported ssNMR spectroscopy. DNP has become a powerful method to enhance spectroscopic sensitivity in high magnetic fields.[6] It has already been applied to selectively enhance surface species in hybrid (bio)materials[7] and to study solvent exposure in membrane proteins.[8]

First, we recorded one-dimensional (1D) ^{13}C and ^{15}N ssNMR experiments using cross polarization (CP, Figure 2 a, c) and direct excitation (DE, Figure 2 b, d) with (black) and without (gray) DNP and determined signal enhancements for ^{13}C, ^{15}N, and ^{29}Si (Section S2.1 in the Supporting Information). 1D ssNMR is sufficient to distinguish different molecular units such as carbohydrates, proteins, and LCPAs (see Table S4). The DNP-enhanced ^{15}N CP ssNMR spectrum (Figure 2 a) showed two signals corresponding to polypeptide backbone nitrogen atoms ($\delta = 120$ ppm) and nitrogen atoms in LCPAs or C_ε of lysine side chains ($\delta = 45$ ppm). The latter signals were considerably reduced without DNP (Figure 2 a, gray). Signals in the ^{15}N DE ssNMR spectrum detected without DNP were weak (Figure 2 b, gray). DNP resulted in selective enhancement of the nitrogen backbone signals at $\delta = 120$ ppm (Figure 2 b), whereas signals from LCPAs or lysine side chains remained absent. ^{13}C ssNMR spectra of *S. turris* biosilica measured with CP and DE (see Figure 2 c and 2 d, respectively) confirmed the presence of all of the organic components.[2] The CP and DE spectra without DNP exhibited prominent signals at about $\delta = 76$ ppm (C2–C6) and 101 ppm (C1), thus indicating the presence of polysaccharides as one major organic species.

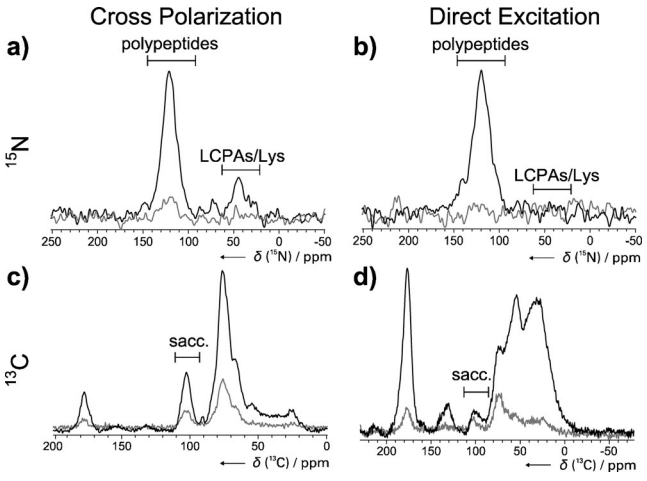

Figure 2. Low-temperature ssNMR spectra of *S. turris* biosilica. a) ^{1}H-^{15}N cross polarization (CP), $\varepsilon = 2$–7; b) ^{15}N direct excitation (DE), $\varepsilon = 20$; c) ^{1}H-^{13}C CP, $\varepsilon = 3.5$–4.4; d) ^{13}C DE, $\varepsilon = 1$–15. The spectra were measured at 400 MHz with DNP (microwaves on, black) and without DNP (microwaves off, gray).

Taken together, our 1D experiments allowed us to identify different molecular species (carbohydrates, proteins, LCPAs)-that exhibit remarkably different DNP enhancement factors ε_N (normalized to the DNP enhancements of the polypeptide signal), as determined from the ratio of ssNMR signal intensities with and without DNP enhancement (Figure 3 a). Peptide signals exhibited the largest enhancements, followed by carbohydrates ($\varepsilon_N = 0.5$), polyamines ($\varepsilon_N = 0.36$), and silicate ($\varepsilon_N = 0.23$). Previous work has shown that DNP enhancements can be used to estimate molecular dimensions on the nanometer scale.[9] The total amount of organic material would correspond to a surface layer of only about 3 nm thickness (see Section S2.2). The largest enhancement factors occur for proteins, thus indicating that these molecules are preferentially located at the solvent-accessible surface. The lower carbohydrate signal enhancements compared with

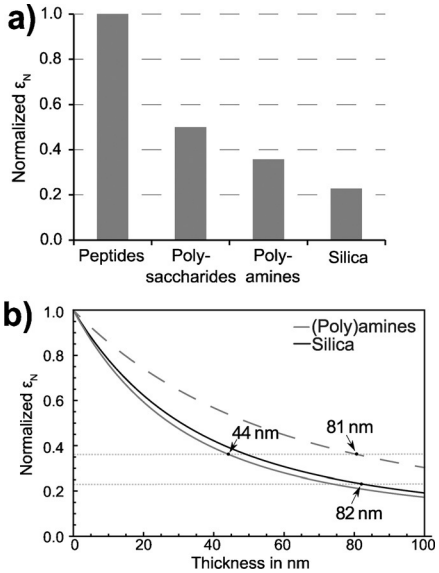

Figure 3. Structural analysis of DNP enhancement factors. a) Measured signal-enhancement factors for biosilica-associated biomolecules normalized to DNP enhancements seen for the protein signal (experimental values given in Table S4). b) Simulated DNP enhancement factors as a function of the thickness of a layer for polyamines and silica. Gray curves represent the normalized enhancement for a theoretically assumed LCPA layer based on reported diffusion constants of 300 nm^2s^{-1} (solid line)[11] and 1000 nm^2s^{-1} (dashed line).[9] The black curve represents the normalized enhancement for silica by using a calculated diffusion constant of 62 nm^2s^{-1} based on an proton–proton distance of 5.5 Å.

proteins may be related to the fact that radicals such as 1-(TEMPO-4-oxy)-3-(TEMPO-4-amino)propan-2-ol (TOTAPOL) preferentially bind to saccharides, which results in paramagnetic quenching. LCPAs are in close contact with the silica[10] and are thus distant from the solvent-accessible surface, which justifies a structural analysis of the DNP parameters. For this purpose, we used a classical spin-diffusion approximation and correlated relative DNP enhancements ε_N seen for LCPAs and silica with the experimentally observed longitudinal nuclear relaxation times (Tables S4, S5). Using spin diffusion constants previously determined for protonated biomolecules[9,11] (see Section S1.6), we obtained an approximate layer thickness of 40–80 nm for the silica–LCPA hybrid material (Figure 3b). Such values are in good agreement with the thickness of the silica structures seen in our microscopy studies (Figure 1c,d) if we assume that the LCPAs are distributed over the entire silica phase. This assumption is reasonable because LCPAs mediate silica precipitation[3a] and diatom biosilica is known to be rather porous and less condensed than other silica materials.[12]

The selective DNP enhancements reported in Figure 2 were confirmed by using AMUPol,[13] which provided higher overall signal enhancements than TOTAPOL[14] (Figure S1 and Table S6) and enabled 2D DNP-supported ssNMR experiments (Figure 4 and Figures S2–S6). Figure 4a,b and Figure 4c display subsections of a ^{13}C-^{15}N correlation spectrum and a ^{15}N-edited ^{13}C-^{13}C correlation experiment, respectively. Intense amine signals occurred at a 40–60 ppm ^{13}C chemical shift and an approximately 45 ppm ^{15}N chemical shift in an NCA-type correlation experiment (Figure 4a), which is characteristic for tertiary amines. In addition, we observed alkyl correlations at a ^{13}C chemical shift of 24 ppm and primary amines with a ^{15}N chemical shift of 33 ppm. These chemical shifts coincide with the LCPA structure proposed previously.[3a] In addition to amines, we detected various signals in the polypeptide backbone (N-CA) region of the ^{13}C-^{15}N correlation spectrum (Figure 4b), the ^{15}N-edited ^{13}C-^{13}C correlation experiment[17] (Figure 4c), and the NCACX data set (Figure 4d). Well-resolved signals appeared especially in the ^{15}N-edited ^{13}C-^{13}C correlation and the NCACX experiment. We compared these experimentally observed 2D correlations to standard secondary chemical shift predictions for all 20 amino acids[15] by using previously defined error margins[16] (colored boxes in Figure 4c,d). This strategy revealed a prominent contribution from aspartic acid (D), glutamic acid (E), glycine (G), serine (S), and alanine (A) residues (see Figures S3, S4 for complete spectra). Remarkably, these ssNMR data were fully confirmed by LC–MS/MS and GC–MS analyses of the samples, which revealed a high abundance of aspartic acid (D), glutamic acid (E), glycine (G), serine (S), and alanine (A) (see Figure 4e and Tables S7, S8). Note that while Figure 4b is in agreement with abundant alanine, we do not find strong alanine correlation peaks in the spectra shown in Figure 4c,d because the low temperature conditions, as observed previously.[7b]

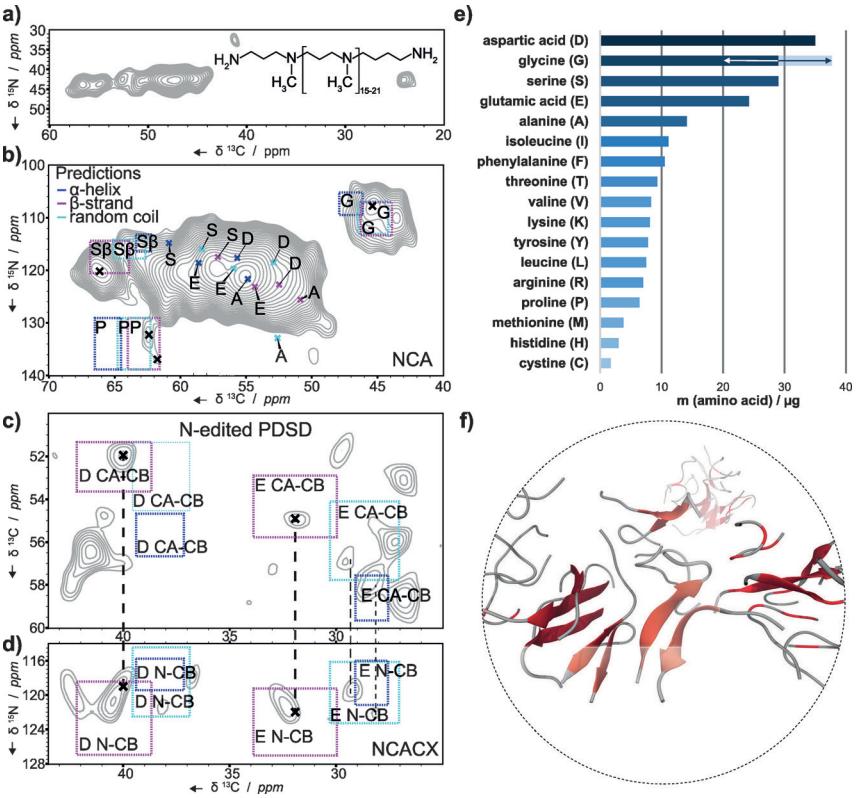

Figure 4. Insight into the amino acid composition and secondary structure of the proteins. a–d) Analysis of 2D ^{13}C-^{15}N correlation experiments measured on a 400 MHz DNP spectrometer. a) Polyamine region of an NCA experiment with the published structure.[3a] b) Protein region with chemical-shift predictions[15,16] for different secondary structures (pink: β-strand, cyan: random coil, blue: α-helix). Boxes represent the standard deviation of chemical-shift predictions for a selected set of amino acids. c,d) Cutouts from 2D experiments of *S. turris* preparations with AMUPol as DNP radical: c) ^{15}N-edited ^{13}C-^{13}C correlation[17] and d) NCACX experiments showing aspartic (D) and glutamic (E) acid Cβ peaks predominantly in β-sheet conformation (for the full spectra see Figures S2–S4). Dashed lines and crosses were introduced for the sake of clarity. e) Quantitative amino acid analysis by LC–MS/MS (Table S7). Note that glycine residues were detected by GC–MS (Table S8). f) Representative snapshot of a MD simulation of 40 model peptides (Ac-DASAGLGDSD-COOH) in aqueous solution.

Next, we analyzed our 2D ssNMR data with respect to protein secondary structure. Proline residues with a Cα shift of approximately 62 ppm occur predominantly in random coil or β-strand conformation (Figure 4b). The presence of serine Cβ (66 ppm, Figure 4b) in β-strand conformation is also likely. Note, however, that the ^{13}C correlations around $\delta =$ 66 ppm can alternatively be explained by α-helical threonine Cα correlations, albeit with less agreement to the experimentally observed ^{15}N chemical shifts. A prominent occurrence of β-strand conformations is also consistent with two different

signals in the glycine region ($\delta = 45$ and 43.5 ppm), which correspond to β-strand/random coil folds ($\delta = 45$ ppm) and protein segments in pronounced β-strand conformation ($\delta =$ 43.5 ppm). Further information was drawn from the ^{15}N-edited ^{13}C-^{13}C correlation and NCACX experiments (Figure 4c,d). Dominant signals occurred in the side-chain region of the abundant aspartic and glutamic acid residues (Figure 4c). Again, the strongest signals were consistent with β-strand conformation.

Taken together, these results suggest that the native silica-associated proteins are dominantly formed by five amino acids and that these residues are mainly found in β-strand and random-coil conformation. Indeed, additional MD simulations (see Section S1.7) for model peptides derived from the measured amino acid composition (see Section S2.5) showed a clear propensity for β-strand secondary structure (Figure 4f). This observation is also in line with earlier in vitro experiments with a recombinant silica-associated protein, rSilC, at liquid–solid and air–solid interfaces.[18] The ssNMR spectra also exhibit prominent signals corresponding to carbohydrates. As described in the Section S2.4, ^{13}C-^{13}C double quantum/single quantum and proton-driven spin diffusion experiments in combination with ^{15}N-edited ^{13}C-^{13}C 2D data revealed the presence of oxygen-linked glucuronic acid as one major saccharide.

In summary, our DNP-ssNMR study delivered structural insight into intact diatom biosilica, a low-surface-area silica/organic hybrid material. The resulting model (Figure 5) involves a surface layer of polysaccharides and proteins that together shield polyamines and silica, which is in line with earlier work indicating the presence of polysaccharides as an outer surface layer.[3h] 2D DNP-ssNMR data allowed us to obtain direct insight into the backbone fold of these native biosilica-associated proteins. The ssNMR analysis in combination with MD simulations suggests a mixture of random-coil and β-strand conformations, which may help to establish compactness as well as intermolecular networking.

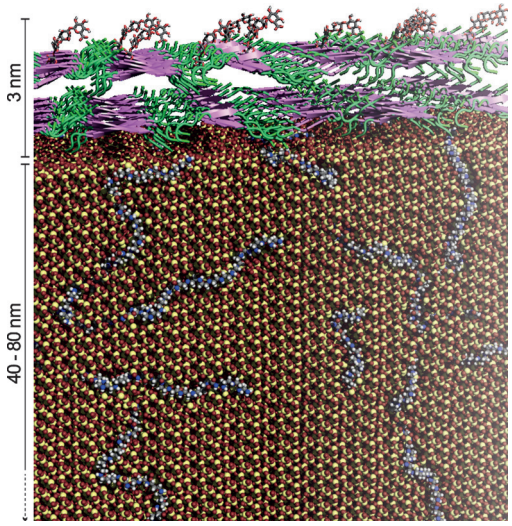

Figure 5. Model for the supramolecular architecture of *S. turris* biosilica. An approximately 3 nm layer containing carbohydrates and proteins covers the 40–80 nm silica phase (colored in red and yellow). The proteins show a tendency to form β-strand secondary structure, as revealed by 2D DNP-ssNMR spectroscopy. Low DNP signals enhancements (ε_N) compared to other detected organic species suggest a broad dispersion of LCPAs (colored in gray, blue, and white) in the silica phase.

Remarkably, both ssNMR and MS suggest that these proteins predominantly contain a selected set of amino acids comprising mainly serine, alanine, glycine, aspartic acid, and glutamic acid. Furthermore, the silica (Figure 5) contains LCPAs. An estimated thickness of about 40–80 nm for the silica/LCPA layer is consistent with our ssNMR results and in agreement with microscopy, which yields a value of approximately 50 nm. On the chemical level, we found clearly resolved signals owing to the *N*-methyl-propyleneimine repetitive unit in the LCPAs (Figure 4a). The polyamine structure determined previously for LCPAs isolated from diatom cell walls could thus be confirmed on intact biosilica.[3a] Lastly, 2D DNP ssNMR showed the presence of an oxygen-linked glucuronic acid as a fraction of the silica-associated carbohydrate material. N-linked saccharides, as well as *N*-acetylglucosamine, can be excluded. Our study underlines the unique possibilities of combining DNP-ssNMR and MS data with MD simulations to study intact complex biomaterials that are difficult to investigate by diffraction methods at both the atomic and nanometer level. The structural information obtained may be useful for the design of novel hybrid materials.

Acknowledgements

This work was conducted within the frameworks of BIONMR, EastNMR and COST (Action TD1103) support programs. We gratefully acknowledge financial support from the Deutsche Forschungsgemeinschaft (FOR 2038, Grant No. BR 1278/24-1) and NWO (grant 722.012.002 to M.W. as well as grants 700.11.344 and 700.26.121 to M.B.). We are indebted to Prof. P. Tordo and his group for providing AMUPol and Prof. N. Kröger (Dresden) for valuable discussions.

Keywords: biomineralization · diatoms · DNP · hybrid materials · solid-state NMR

How to cite: *Angew. Chem. Int. Ed.* **2015**, *54*, 15069–15073
Angew. Chem. **2015**, *127*, 15284–15288

[1] C. Jeffryes, S. N. Agathos, G. Rorrer, *Curr. Opin. Biotechnol.* **2015**, *33*, 23–31.
[2] C. Gröger, K. Lutz, E. Brunner, *Prog. Nucl. Magn. Reson. Spectrosc.* **2009**, *54*, 54–68.
[3] a) N. Kröger, R. Deutzmann, C. Bergsdorf, M. Sumper, *Proc. Natl. Acad. Sci. USA* **2000**, *97*, 14133–14138; b) N. Kröger, R. Deutzmann, M. Sumper, *Science* **1999**, *286*, 1129–1132; c) S. Wenzl, R. Hett, P. Richthammer, M. Sumper, *Angew. Chem. Int. Ed.* **2008**, *47*, 1729–1732; *Angew. Chem.* **2008**, *120*, 1753–1756; d) A. Scheffel, N. Poulsen, S. Shian, N. Kröger, *Proc. Natl. Acad. Sci. USA* **2011**, *108*, 3175–3180; e) R. E. Hecky, K. Mopper, P. Kilham, E. T. Degens, *Mar. Biol.* **1973**, *19*, 323–331; f) A. Chiovitti, R. E. Harper, A. Willis, A. Bacic, P. Mulvaney, R. Wetherbee, *J. Phycol.* **2005**, *41*, 1154–1161; g) R. Hedrich, S. Machill, E. Brunner, *Carbohydr. Res.* **2013**, *365*, 52–60; h) B. Tesson, M. Hildebrand, *PLoS ONE* **2013**, *8*, e61675.

[4] A. Roehrich, G. Drobny, *Acc. Chem. Res.* **2013**, *46*, 2136 – 2144.
[5] a) C. Bonhomme, C. Gervais, D. Laurencin, *Prog. Nucl. Magn. Reson. Spectrosc.* **2014**, *77*, 1 – 48; b) B. Tesson, S. Masse, G. Laurent, J. Maquet, J. Livage, V. Martin-Jézéquel, T. Coradin, *Anal. Bioanal. Chem.* **2008**, *390*, 1889 – 1898; c) M. J. Duer, *J. Magn. Reson.* **2015**, *253*, 98 – 110; d) S. Kababya, A. Gal, K. Kahil, S. Weiner, L. Addadi, A. Schmidt, *J. Am. Chem. Soc.* **2015**, *137*, 990 – 998; e) G. Goobes, R. Goobes, O. Schueler-Furman, D. Baker, P. S. Stayton, G. P. Drobny, *Proc. Natl. Acad. Sci. USA* **2006**, *103*, 16083 – 16088; f) Y.-Y. Hu, A. Rawal, K. Schmidt-Rohr, *Proc. Natl. Acad. Sci. USA* **2010**, *107*, 22425 – 22429.
[6] a) L. R. Becerra, G. J. Gerfen, R. J. Temkin, D. J. Singel, R. G. Griffin, *Phys. Rev. Lett.* **1993**, *71*, 3561 – 3564; b) D. A. Hall, D. C. Maus, G. J. Gerfen, S. J. Inati, L. R. Becerra, F. W. Dahlquist, R. G. Griffin, *Science* **1997**, *276*, 930 – 932; c) A. B. Barnes, G. D. Paëpe, P. C. A. v. d. Wel, K.-N. Hu, C.-G. Joo, V. S. Bajaj, M.-L. Mak-Jurkauskas, J. R. Sirigiri, J. Herzfeld, R. J. Temkin, R. G. Griffin, *Appl. Magn. Reson.* **2008**, *34*, 237 – 263; d) M. Kaplan, A. Cukkemane, G. C. P. van Zundert, S. Narasimhan, M. Daniëls, D. Mance, G. Waksman, A. M. J. J. Bonvin, R. Fronzes, G. E. Folkers, M. Baldus, *Nat. Methods* **2015**, *12*, 649 – 652.
[7] a) A. Lesage, M. Lelli, D. Gajan, M. A. Caporini, V. Vitzthum, P. Miéville, J. Alauzun, A. Roussey, C. Thieuleux, A. Mehdi, G. Bodenhausen, C. Coperet, L. Emsley, *J. Am. Chem. Soc.* **2010**, *132*, 15459 – 15461; b) E. J. Koers, M. P. López-Deber, M. Weingarth, D. Nand, D. T. Hickman, D. M. Ndao, P. Reis, A. Granet, A. Pfeifer, A. Muhs, M. Baldus, *Angew. Chem. Int. Ed.* **2013**, *52*, 10905 – 10908; Angew. Chem. **2013**, 125, 11106 – 11109.
[8] E. J. Koers, E. A. W. van der Cruijsen, M. Rosay, M. Weingarth, A. Prokofyev, C. Sauvée, O. Ouari, J. van der Zwan, O. Pongs, P. Tordo, W. E. Maas, M. Baldus, *J. Biomol. NMR* **2014**, *60*, 157 – 168.
[9] P. C. A. van der Wel, K.-N. Hu, J. Lewandowski, R. G. Griffin, *J. Am. Chem. Soc.* **2006**, *128*, 10840 – 10846.
[10] D. Wisser, S. I. Brückner, F. M. Wisser, G. Althoff-Ospelt, J. Getzschmann, S. Kaskel, E. Brunner, *Solid State Nucl. Magn. Reson.* **2015**, *66 – 67*, 33 – 39.
[11] C. Ader, R. Schneider, K. Seidel, M. Etzkorn, S. Becker, M. Baldus, *J. Am. Chem. Soc.* **2009**, *131*, 170 – 176.
[12] E. G. Vrieling, Q. Sun, M. Tian, P. J. Kooyman, W. W. C. Gieskes, R. A. v. Santen, N. A. J. M. Sommerdijk, *Proc. Natl. Acad. Sci. USA* **2007**, *104*, 10441 – 10446.
[13] C. Sauvée, M. Rosay, G. Casano, F. Aussenac, R. T. Weber, O. Ouari, P. Tordo, *Angew. Chem. Int. Ed.* **2013**, *52*, 10858 – 10861; *Angew. Chem.* **2013**, *125*, 11058 – 11061.
[14] C. Song, K.-N. Hu, C.-G. Joo, T. M. Swager, R. G. Griffin, *J. Am. Chem. Soc.* **2006**, *128*, 11385 – 11390.
[15] Y. Wang, O. Jardetzky, *Protein Sci.* **2002**, *11*, 852 – 861.
[16] K. Seidel, M. Etzkorn, R. Schneider, C. Ader, M. Baldus, *Solid State Nucl. Magn. Reson.* **2009**, *35*, 235 – 242.
[17] L. A. Baker, M. Daniëls, E. A. W. van der Cruijsen, G. E. Folkers, M. Baldus, *J. Biomol. NMR* **2015**, *62*, 199 – 208.
[18] E. Kharlampieva, C. M. Jung, V. Kozlovskaya, V. V. Tsukruk, *J. Mater. Chem.* **2010**, *20*, 5242 – 5250.

Received: August 6, 2015
Published online: October 28, 2015

